Measurement of L-shell electron-impact ionization cross sections for highly charged uranium ions

Th. Stöhlker and A. Krämer
University of Frankfurt, D-60486 Frankfurt, Germany
and Gesellschaft für Schwerionenforschung, D-64220 Darmstadt, Germany

S. R. Elliott,* R. E. Marrs, and J. H. Scofield
Lawrence Livermore National Laboratory, Livermore, California 94551
(Received 13 January 1997)

L-shell electron-impact ionization cross sections for highly charged uranium ions from fluorinelike U^{83+} through lithiumlike U^{89+} have been measured at 45-, 60-, and 75-keV electron energy. The cross sections were obtained from x-ray measurements of the equilibrium ionization balance in an electron beam ion trap. The measured cross sections agree with recent relativistic distorted wave calculations. [S1050-2947(97)07109-6]

PACS number(s): 34.80.Kw, 32.30.Rj

I. INTRODUCTION

Electron-impact ionization is a fundamental process in the physics of electron-ion collisions. Although cross-section measurements are available for ions in low charge states, there have been very few measurements of electron-impact ionization cross sections for very highly charged ions. Recently, we reported the first measurements of electron-impact ionization cross sections for the hydrogenlike ions of several high-Z elements ranging from molybdenum ($Z=42$) to uranium ($Z=92$) [1,2]. These measurements provided the first accurate cross section information for the ionization of very highly charged ions, and determined the reliability of theoretical calculations for K-shell ionization. In the present work, we report similar results for the ionization of L-shell electrons, for which the thresholds are lower and the ionization cross sections larger than those for K-shell ionization. In this paper we report measurements of L-shell electron-impact ionization cross sections for the seven highly charged uranium ions from fluorinelike U^{83+} through lithiumlike U^{89+}.

II. EXPERIMENTAL METHOD

The present measurements were done using an extension of the ionization-balance technique that we used previously to measure electron-impact ionization cross sections for hydrogenlike ions [1]. The present experimental arrangement is nearly identical to that in Ref. [1], where additional details can be found. Highly charged uranium ions were produced and trapped in the high-energy electron-beam ion trap at the Lawrence Livermore National Laboratory [3]. In this device, ions are trapped by the space-charge potential of the electron beam and held within the beam for times much longer than the time required to strip uranium ions to very high charge states. Hence the ionization balance reaches a steady-state equilibrium. Radiative recombination (RR) x rays from capture of beam electrons into the partially filled L shell of trapped uranium ions were used to determine the relative abundance of the different uranium charge states present in the trap. Ionization cross sections were then determined from the measured abundances.

The processes that affect the charge-state distribution of the trapped uranium ions are electron-impact ionization, radiative recombination, and charge-exchange recombination with neutral gas. Although neutral gas is undesirable because of its effect on the uranium ionization balance, neutral neon atoms were intentionally injected into the trap in order to provide a source of low-Z ions for evaporative cooling of the highly charged uranium ions. Evaporative cooling is necessary to keep the uranium ions trapped within the electron beam [4].

Single-electron-impact ionization and radiative recombination are the only electron-beam-induced processes that affect the ionization balance. The cross section for multiple ionization, in which two electrons are removed from the target by a single incident electron, is negligible for the highly ionized uranium ions that are the subject of the present work. Excitation autoionization requires an (energetically forbidden) inner-shell excitation, and resonant processes such as resonant excitation and dielectronic recombination do not occur at the beam energies used in the present work.

In equilibrium, the abundance ratio of any two adjacent uranium charge states, denoted by q and $q+1$, is determined by the ionization and recombination cross sections connecting them:

$$\frac{N_q}{N_{q+1}} = \frac{\sigma^{\mathrm{RR}}_{q+1} + \langle \sigma^{\mathrm{CX}}_{q+1} \rangle}{\sigma^{\mathrm{ion}}_{q}} . \tag{1}$$

Here the ionization and RR cross sections are denoted by σ^{ion} and σ^{RR}, respectively, and $\langle \sigma^{\mathrm{CX}} \rangle$ is an effective charge-exchange-recombination cross section given by $\langle \sigma^{\mathrm{CX}} \rangle = (e/j_e) n_0 v \sigma^{\mathrm{CX}}$, where e is the electron charge, n_0 is the neutral gas density, v is the ion-neutral collision velocity (approximately the ion thermal velocity), and σ^{CX} is the actual charge-exchange-recombination cross section. The ef-

*Present address: Department of Physics, University of Washington, Seattle, WA 98195.

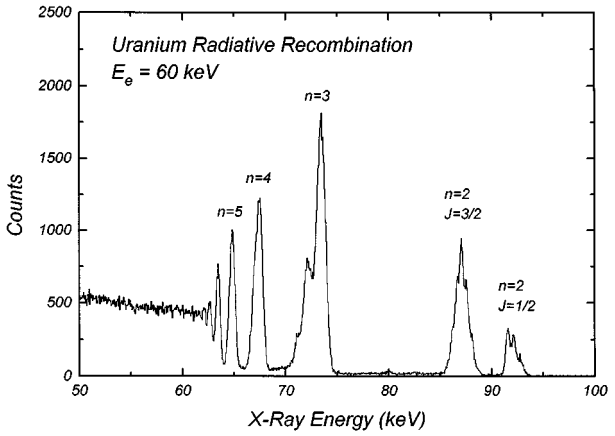

FIG. 1. Radiative-recombination x-ray spectrum for uranium ions at 60-keV electron energy. Capture into the L shell is split into $J=\frac{1}{2}$ and $\frac{3}{2}$ components, each of which contains partially resolved lines from the different ion charge states present in the trap.

fective current density j_e includes the overlap between trapped uranium ions and the electron beam. The dimensionless quantity $(e/j_e)n_0 v$ is much less than 1, and $\langle \sigma^{\mathrm{CX}} \rangle$ is smaller than σ^{RR}. The ionization cross section σ_q^{ion} for each charge state can be determined from Eq. (1) if the other quantities are known. To accomplish this, we determine N_q/N_{q+1} spectroscopically, use calculated values of σ^{RR}, and determine a correction for $\langle \sigma^{\mathrm{CX}} \rangle$ as described below. We calculated RR cross sections using an accurate relativistic treatment as described in Ref. [1].

A. X-ray measurements

A 1-cm-thick planar germanium detector positioned at 90° to the electron beam was used to obtain spectra of RR x rays from uranium target ions in the trap. A spectrum obtained at 60-keV electron energy is shown in Fig. 1. Similar spectra were obtained at electron energies of 45 and 75 keV. The x-ray spectra consist of a series of peaks corresponding to RR into the open shells of the uranium target ions. RR into the higher Rydberg levels joins smoothly with bremsstrahlung radiation at an x-ray energy equal to the electron-beam energy.

Uranium was injected into the trap as low-charge-state ions from a vacuum spark source [5]. Outer, loosely bound electrons are removed by the electron beam very quickly, and the uranium ions reach an equilibrium charge-state distribution determined according to Eq. (1). X rays were counted for six 5-s time periods beginning 1.6 s after the initial injection of uranium into the trap. Many such counting cycles were combined to accumulate a final set of six time routed spectra at each electron energy. RR peak ratios in the six routed spectra were compared to determine whether the ionization balance was in equilibrium. There is evidence that the uranium was slightly less ionized in the first spectrum than in the others, as expected from an estimate of the ionization times, so the first spectrum was discarded and spectra two through six were summed together for further analysis. The absolute uranium count rate fell by about 3% during the 30-s counting period. This small loss rate for uranium ions, which is approximately the same for adjacent charge states, is too small to affect the ionization balance in the trap.

B. Charge-state distribution

X-ray emission from RR into the partially filled L shell of the trapped uranium ions reveals information about their charge state. The spin-orbit splitting of roughly 4.5 keV between $J=\frac{3}{2}$ and $\frac{1}{2}$ levels in the uranium L shell produces two broad peaks in the RR x-ray spectra (see Fig. 1). The shift in ionization potential as the uranium-ion charge changes by one unit is roughly equal to the resolution of our detector, producing a series of partially resolved RR lines within each of the broad peaks as indicated in Fig. 2, where the L-shell RR spectra at each of the three electron energies are shown. The ionization balance shifts toward higher charge states as the electron energy increases because the ionization cross section increases and the RR cross section decreases with increasing electron energy.

1. Spectrum fitting

The count rate in each RR line is proportional to the differential RR cross section at 90° times the abundance of the corresponding target ion in the trap. Absolute RR cross sections can be calculated with an accuracy of 3% or better [1,6], and relative cross sections even more accurately, so we used the calculated differential RR cross sections in a least-squares fitting procedure to determine the charge-state distribution of the uranium ions. The relative energies of the RR lines (i.e., the ion energy levels) were fixed at values calculated with a relativistic Hartree-Fock method. An overall energy offset (the electron beam energy) was left as a free parameter. In those cases where more than one final state is populated in RR on the same target ion, the relative amplitudes were frozen at the theoretical values during the fitting procedure.

The RR spectra were fitted with a line shape consisting of a Gaussian peak plus a shelf on the low-energy side. The accuracy of this line shape was corroborated by fitting high-statistics lines from radioactive sources. Pileup tails are insignificant in our spectra, as verified by examining the shape of a pulser peak accumulated simultaneously with the uranium x rays. The $J=\frac{3}{2}$ and $\frac{1}{2}$ RR peaks were fitted simultaneously, with the relative amplitudes for lines from the same target ion held fixed. The efficiency of the detector does not change significantly over the 4.5-keV energy separation between the two peaks. Different x-ray linewidths were allowed for the $J=\frac{3}{2}$ and $\frac{1}{2}$ peaks, but the separate RR lines within each peak were constrained to have the same width. As a consistency check, the $J=\frac{3}{2}$ and $\frac{1}{2}$ peaks were fitted separately: Changes in the fitted intensities of less than 3% were observed for all charge states except for the low-abundance lithiumlike and heliumlike charge states, from which the RR signals are weak.

The $(2s_{1/2}2p_{1/2})_{J=0}$ metastable level in berylliumlike uranium is expected to have a lifetime on the order of 10^3 s, and may have an observable abundance in our trap. The berylliumlike metastable was fitted as a separate target-ion species, but the small (5–10 %) fitted abundance obtained for it was then combined with the berylliumlike ground state abundance for cross section analysis.

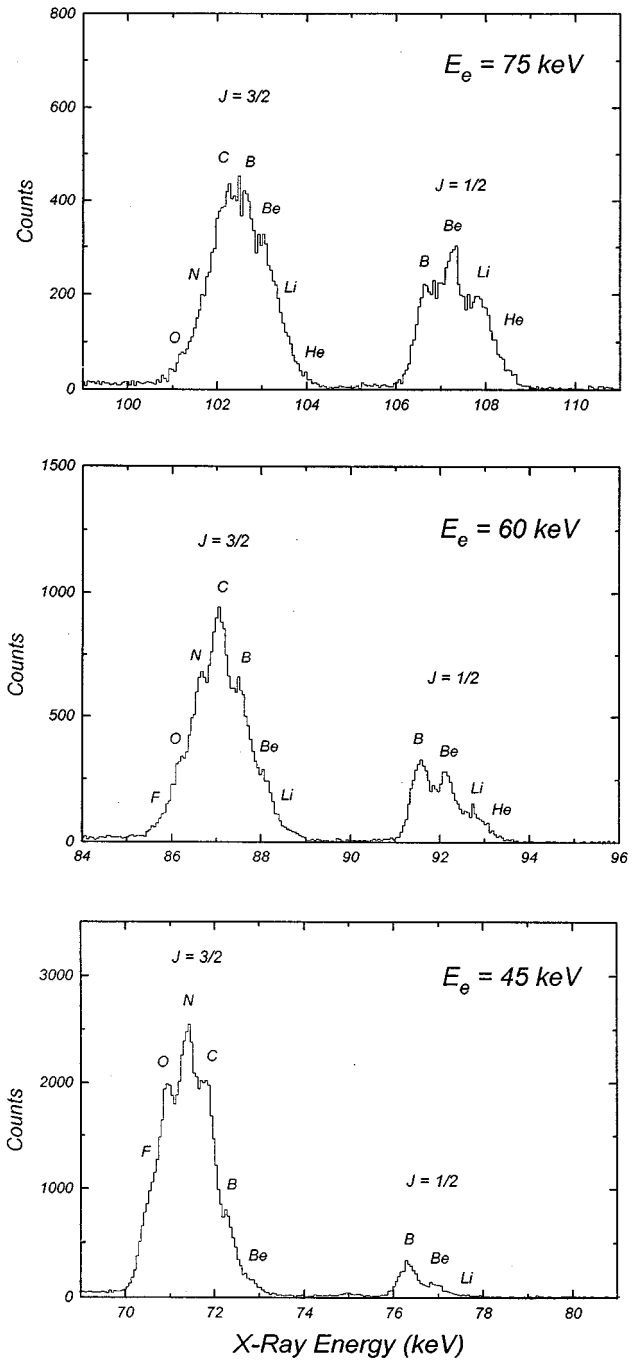

FIG. 2. Uranium L-shell RR at each of the three electron energies. The chemical symbols indicate the approximate position of RR lines from the corresponding uranium target ions.

2. Absorption-edge measurements

Although the roughly 450-eV full width at half maximum resolution in our RR ($n=2$) x-ray spectra is sufficient to allow the intensities of the RR lines from different uranium charge states to be determined as described above, we used an absorption edge technique to help confirm that our understanding of the RR x-ray spectra is correct. At 60-keV electron energy, the energies of L-shell RR x rays from uranium are close to the 88.0-keV K edge of lead [7] (see Fig. 1). Since the width of the K edge in lead is several times less than the resolution of our germanium detector, a cleaner

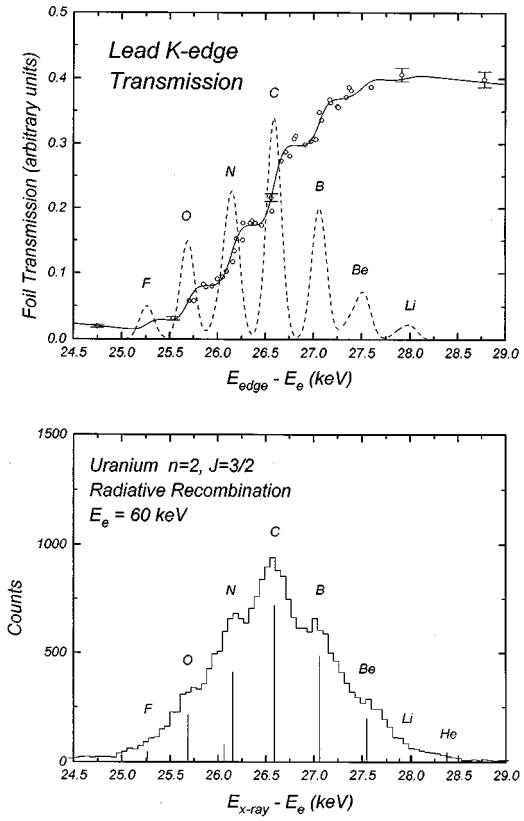

FIG. 3. Comparison of the structure in the $J=\frac{3}{2}$ RR peak as seen by scanning the RR energy across the K absorption edge of lead and as seen in the germanium detector at fixed electron energy. Chemical symbols refer to the different target-ion charge states as in Fig. 2. Top: Ratio of x-ray counts with and without a lead foil in front of the detector. Typical error bars are shown. The solid curve is a least-squares fit as explained in the text, and the broken curve is its first derivative. Bottom: The germanium detector spectrum at 60-keV electron energy with no absorber. The vertical lines indicate the position and relative strength of the RR lines from each target ion. The energy scales for the top and bottom frames are identical and equivalent to the binding energy of the captured electron.

separation of RR lines from the different uranium charge states might be obtained with absorption-edge spectroscopy. We used small changes in the electron-beam energy (near 60 keV) to walk the position of the $n=2$, $J=\frac{3}{2}$ RR peak across the lead absorption edge. The count rate for this peak in a second germanium detector covered with a 0.6-mm-thick lead foil was recorded as a function of beam energy, and the first detector was used for normalization. For this foil the ratio of x-ray transmission at energies just above and below the lead K edge is 0.018, which essentially extinguishes each line as it is moved above the edge. To improve the accuracy of the electron energy scale and reduce the effects of possible drifts in the high voltage power supplies or changes in the space-charge potential in the trap, electron energies were determined from the centroid of the RR ($n=4$) x-ray peak.

The measured x-ray transmission through the lead absorber foil is shown in the top panel of Fig. 3 as a function of the energy difference between the absorption edge and the electron energy. This energy difference is equal to the binding energy of the captured electron. The solid curve in Fig. 3 is the result of a least-squares fit which was obtained with an

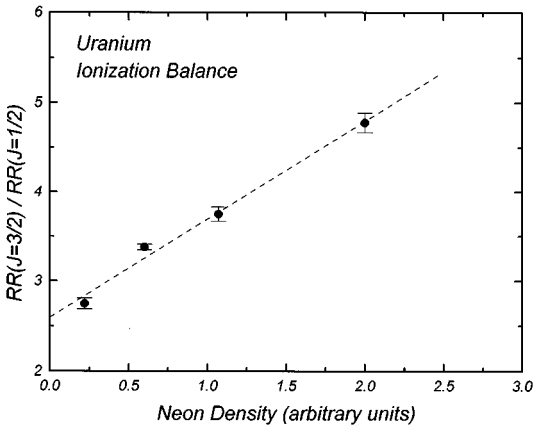

FIG. 4. The effect of neutral neon density on the uranium ionization balance as indicated by the observed ratio of L-shell RR into $J=\frac{3}{2}$ and $\frac{1}{2}$ orbitals. The broken line is a best guess at the true density dependence; its slope was used to determine the amount of charge-exchange recombination as explained in the text.

error-function representation of the lead absorption edge [8] and with the theoretical transition energies for RR into the $J=\frac{3}{2}$ levels of the various target-ion species. The broken curve is the first derivative of the solid curve; it shows the resolution and position for the different capture lines. The width of the absorption edge was a free parameter in the fitting procedure. It includes contributions from the electron-beam energy spread and the true width of the lead K edge. The bottom panel of Fig. 3 shows the 60-keV germanium-detector spectrum for the $J=\frac{3}{2}$ RR peak, along with the position and strength of the fitted RR lines. As can be seen by comparing the two panels in Fig. 3, the higher-resolution absorption-edge data are consistent with the spectrum of RR lines fitted to the germanium-detector data.

C. Charge-exchange recombination

After the ionization balance [N_q/N_{q+1} in Eq. (1)] has been determined from fits to the x-ray spectra, the remaining piece of information required to obtain ionization cross sections is the effective charge-exchange-recombination cross section with neutral gas $\langle\sigma^{\mathrm{CX}}\rangle$. (Charge exchange between a highly charged uranium ion and any other ion is negligible at the low kinetic energies of the ions in our trap because Coulomb repulsion limits the distance of closest approach.) Although $\langle\sigma^{\mathrm{CX}}\rangle$ is much smaller than σ^{RR} [see Eq. (1)], and could even be neglected for some of the target ions, we have attempted to determine its value as accurately as possible.

1. Effect of neutral gas

As mentioned above, it is necessary to inject neutral (neon) gas into our trap in order to supply light ions for the evaporative cooling process. The resultant charge-exchange recombination affects the equilibrium ionization balance of the uranium ions as given in Eq. (1). We correct for charge-exchange recombination by running at several different neutral densities and extrapolating the effect to zero. This is the same technique used previously to account for charge-exchange recombination in the measurement of hydrogenlike ionization cross sections [1].

TABLE I. Calculated total RR cross sections for U^{84+} (oxygen-like) through U^{90+} (heliumlike) at the three electron energies used for ionization cross section measurements. Cross-section units are 10^{-24} cm^2.

Target ion	45 keV	60 keV	75 keV
O-like	122.4	74.4	50.1
N-like	137.5	83.3	56.0
C-like	148.4	89.8	60.3
B-like	174.0	105.9	71.3
Be-like	195.7	119.6	80.8
Li-like	224.6	139.5	95.5
He-like	250.1	157.3	108.8

The 45-, 60-, and 75-keV spectra from which ionization cross sections were obtained were all acquired at the same electron current (200 mA) and the same neutral density, so the effective charge-exchange-recombination cross section $\langle\sigma^{\mathrm{CX}}\rangle$ is the same at all three energies. At one of the energies (60 keV) several runs were taken at different neutral densities and different electron current densities to determine the amount of charge-exchange recombination. At low neutral density, where charge exchange is minimized, the count rate is too low to obtain an accurate ionization balance from which ionization cross sections can be determined. However, the ratio of total counts in the $J=\frac{3}{2}$ and $\frac{1}{2}$ peaks, which can be determined accurately even at low neutral densities, is a good measure of the effect of charge-exchange recombination, and we use this ratio to determine $\langle\sigma^{\mathrm{CX}}\rangle$.

2. X-ray intensity ratios

The RR($J=\frac{3}{2}$) and RR($J=\frac{1}{2}$) intensities are the sums of the product of the RR cross sections and abundances for all the different target ions in the trap. The RR($J=\frac{1}{2}$) peak is dominated by contributions from boronlike and berylliumlike target ions, while the RR($J=\frac{3}{2}$) peak is dominated by contributions from nitrogenlike, carbonlike, and boronlike target ions. Charge exchange causes a shift of the ionization balance toward lower charge, affecting the intensities of the two peaks. The intensity ratio RR($J=\frac{3}{2}$)/RR($J=\frac{1}{2}$), denoted in what follows by R, is expected to be very close to a linear function of the neutral gas density, at least for the small range of gas densities used here. An examination of the details of the ionization balance shows that the ratio R is roughly proportional to the abundance ratio N_q/N_{q+1}, where the index q refers to any of the most abundant uranium charge states. Following Eq. (1), we expect

$$R\propto\frac{N_q}{N_{q+1}}=(1/\sigma_q^{\mathrm{ion}})\left[\sigma_{q+1}^{\mathrm{RR}}+\frac{K_{\mathrm{Ne}}n_{\mathrm{Ne}}}{j_e}+\frac{K_{\mathrm{Bkg}}n_{\mathrm{Bkg}}}{j_e}\right],\quad(2)$$

where n_{Ne} and n_{Bkg} are the densities of neutral neon and unknown background gasses, respectively, and K_{Ne} and K_{Bkg} are constants. The second and third terms are the effective charge-exchange-recombination cross sections for injected neon and background gas, respectively. A plot of the measured neutral-density dependence of R at 60 keV and 200-mA electron-beam current is shown in Fig. 4. As ex-

TABLE II. Measured ionization cross sections for U^{83+} (fluorinelike) through U^{89+} (lithiumlike). At each electron energy the theoretical relativistic distorted wave cross sections from Ref. [11] and the ratio of experiment and theory are also given. Cross-section units are 10^{-24} cm^2. The shift of the uranium ionization balance with electron energy (see Fig. 2) precluded cross-section measurements for lithiumlike uranium at 45 keV and fluorinelike uranium at 75 keV.

Ionization stage	45 keV Expt.	45 keV Theory	45 keV Expt./Theory	60 keV Expt.	60 keV Theory	60 keV Expt./Theory	75 keV Expt.	75 keV Theory	75 keV Expt./Theory
F-like	178±19	162	1.10±0.12	241±42	183	1.32±0.23			
O-like	141±14	125	1.13±0.11	164±24	145	1.13±0.17	171±36	151	1.13±0.24
N-like	114±11	90	1.27±0.12	144±20	109	1.32±0.18	179±34	115	1.56±0.30
C-like	68±6	58	1.17±0.10	91±11	75	1.21±0.15	97±16	81	1.20±0.20
B-like	50±5	39	1.28±0.12	68±8	52	1.31±0.16	80±13	56	1.43±0.22
Be-like	23.5±3.6	22.2	1.06±0.16	41.5±4.7	30.4	1.37±0.15	43.3±6.2	33.1	1.31±0.19
Li-like				18.4±3.1	14.7	1.25±0.21	18.9±3.1	16.1	1.17±0.19

pected, the behavior is roughly linear. The broken line is a best guess at the true dependence on neon density. Its slope determines the value of the constant K_{Ne}, and the $n_{\mathrm{Ne}}=0$ intercept (at $R=2.6$) gives the value of R in the absence of charge exchange with neon atoms.

In order to account for the possible presence of neutral species in the trap that are unrelated to the neon gas injection and may even be a different species, such as hydrogen, we repeated the neon-density-dependence measurements at electron currents of 135, 100, and 75 mA. Since the electron current density is proportional to the total current (because the beam radius is constant), these measurements give the dependence of R on the current density j_e, and provide an estimate of the quantity $K_{\mathrm{Bkg}}n_{\mathrm{Bkg}}$. The results imply that charge exchange with background gas is a small effect. This procedure gives an estimated value of $R=2.2$ in the complete absence of charge exchange, as compared with $R=3.38$ at the neon density used for our cross section measurements (0.6 on the scale of Fig. 4).

3. Effective charge-exchange cross section

The effective charge-exchange cross section $\langle\sigma^{\mathrm{CX}}\rangle$ was obtained from an ionization-balance model as follows: First, we anticipate (correctly) that the actual ionization cross sections will not have pathological variations among the different uranium charge states and will look like the theoretical values times a scale factor. We then find the cross-section scale factor that results in an ionization balance that yields the no-charge-exchange value of $R=2.2$ (when combined with the known RR cross sections). Next, we assume that the charge-exchange-recombination cross sections are simply proportional to q, as suggested by other measurements [9,10], and find the normalization factor for the charge-exchange cross sections that increases the value of R to that observed in the runs used for measuring ionization cross sections ($R=3.38$). The resulting values of $\langle\sigma^{\mathrm{CX}}\rangle$ for $q=83-89$ range from 32 to 34×10^{-24} cm^2, which should be compared with the much larger RR cross sections listed in Table I. These values of $\langle\sigma^{\mathrm{CX}}\rangle$ and the RR cross sections from Table I were used in Eq. (1) to obtain ionization cross sections. In all cases, recombination is dominated by RR. We conservatively assign an error of 50% to $\langle\sigma^{\mathrm{CX}}\rangle$ based on estimates of the precision of the extrapolation procedure and the possible effect of neglected multiple charge exchange.

Note that the effect of the charge-exchange correction is to (linearly) extrapolate the rate of neutral-gas-dependent recombination to zero neutral density and eliminate it. This procedure is relatively insensitive to the amount of multiple charge exchange (i.e., capture of more than one electron from a neutral atom). The main effect of multiple charge exchange is to make the single-charge-exchange term $\langle\sigma^{\mathrm{CX}}\rangle$ appear larger than it would otherwise. An exact treatment of multiple charge exchange, which couples the abun-

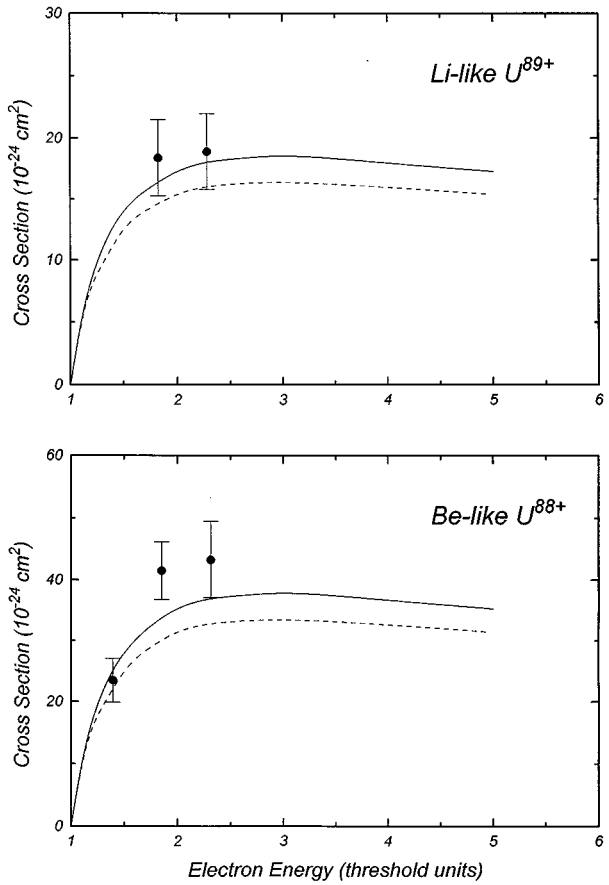

FIG. 5. Measured electron-impact ionization cross section for lithiumlike and berylliumlike uranium compared to relativistic distorted wave theory as given in Ref. [14]. The solid curve is theory with the Moeller interaction, and the dashed curve is theory with the Coulomb interaction only.

dances of more than two uranium charge states, is not justified in view of the relatively low rate of charge exchange in the present experiment.

III. IONIZATION CROSS SECTIONS

Separate ionization cross sections for each target ion were obtained with Eq. (1) using the abundance ratios for adjacent charge states obtained from the least-squares fits to the x-ray spectra, theoretical RR cross sections, and effective charge-exchange-recombination cross sections as explained above. The results are presented in Table II. The listed uncertainties are the quadrature sum of the uncertainties in $\langle \sigma^{\mathrm{CX}} \rangle$, N_q, and N_{q+1}. The estimated 3% uncertainty in the RR cross sections used for normalization (see Table I) is not included. (There is an additional error of less than 2% in the RR cross sections due to the fact that they were calculated at the nominal electron energies of 45, 60, and 75 keV, while the actual energies were 45.2, 60.4, and 75.6 keV as determined from the measured x-ray spectra.) If we had not made a correction for charge-exchange recombination, our measured electron-impact ionization cross sections would be smaller by amounts ranging from 13% (for berylliumlike uranium at 45 keV) to 37% (for oxygenlike uranium at 75 keV).

Reduced cross sections for electron-impact ionization were calculated by Zhang and Sampson using relativistic distorted wave theory with a Coulomb interaction between the electrons [11]. We evaluated these theoretical cross sections for the electron energies and target ions used in the present work, and they are listed in Table II for comparison with the measured cross sections. Our measured cross sections are systematically larger than these theoretical values. However, it should be pointed out that the experimental values and their uncertainties are correlated due to the similar charge-exchange correction applied to all of them.

As a result of our previous measurements of K-shell ionization cross sections for high-Z ions [1], and corresponding theoretical calculations that explored the importance of the Moeller (i.e., first-order QED) interaction [12,13], it was discovered that the actual K-shell ionization cross sections are substantially larger than those calculated with only a Coulomb interaction as in Ref. [11]. Moores and Reed calculated the L-shell electron-impact ionization cross section for lithiumlike and berylliumlike uranium with and without the Moeller interaction [14]. A comparison between their results and the present measurements is shown in Fig. 5. As expected, the theory with the Moeller interaction is closer to our measured cross sections than the theory with the Coulomb interaction only. However the difference between the two types of calculations is much less than at the higher electron energies required for K-shell ionization.

Although we listed measured cross sections for seven different uranium ions in Table II, there are really only three independent physical quantities. These are the reduced cross sections for ionization of the $2s_{1/2}$, $2p_{1/2}$, and $2p_{3/2}$ subshells. The actual cross sections for the different uranium ions are expected to be proportional to the number of bound electrons in each subshell times the appropriate reduced cross section. The theoretical cross sections in Table II were computed from the three (theoretical) reduced cross sections, and the fact that there is a fairly uniform difference between theory and experiment across the span of seven charge states suggests that the relative size of the theoretical reduced cross sections is correct.

IV. SUMMARY AND CONCLUSIONS

Cross sections for L-shell electron-impact ionization of highly charged uranium ions have been measured at three different electron energies, and the results support relativistic distorted wave calculations that include the Moeller interaction. The present results can be combined with our previous measurements of K-shell ionization cross sections to form a consistent picture of the ionization of very-highly-charged ions. In both cases the measurements span the electron energy range up to a few times threshold and agree with theoretical calculations that include both the Moeller interaction and exchange.

ACKNOWLEDGMENTS

This work was supported in part by the Office of Basic Energy Sciences, Division of Chemical Sciences, U.S. Department of Energy, and was performed under the auspices of the U.S. Department of Energy by the Lawrence Livermore National Laboratory under Contract No. W-7405-Eng-48.

[1] R. E. Marrs, S. R. Elliott, and J. H. Scofield, Phys. Rev. A **56**, 1338 (1997).
[2] R. E. Marrs, S. R. Elliott, and D. A. Knapp, Phys. Rev. Lett. **72**, 4082 (1994).
[3] D. A. Knapp, R. E. Marrs, S. R. Elliott, E. W. Magee, and R. Zasadzinski, Nucl. Instrum. Methods Phys. Res. A **334**, 305 (1993).
[4] M. A. Levine, R. E. Marrs, J. R. Henderson, D. A. Knapp, and M. B. Schneider, Phys. Scr. **T22**, 157 (1988).
[5] I. G. Brown, J. E. Galvin, R. A. MacGill, and R. T. Wright, Appl. Phys. Lett. **49**, 1019 (1986).
[6] J. H. Scofield, Phys. Rev. A **40**, 3054 (1989).
[7] A. J. Bearden, Phys. Rev. Lett. **4**, 240 (1960).
[8] J. H. Lupton, D. D. Dietrich, C. J. Hailey, R. E. Stewart, and K. P. Ziock, Phys. Rev. A **50**, 2150 (1994).
[9] A. Müller and E. Salzborn, Phys. Lett. **62A**, 391 (1977).
[10] B. R. Beck, J. Steiger, G. Weinberg, D. A. Church, J. McDonald, and D. Schneider, Phys. Rev. Lett. **77**, 1735 (1996).
[11] H. L. Zhang and D. H. Sampson, Phys. Rev. A **42**, 5378 (1990).
[12] C. J. Fontes, D. H. Sampson, and H. L. Zhang, Phys. Rev. A **51**, R12 (1995).
[13] D. L. Moores and K. J. Reed, Nucl. Instrum. Methods Phys. Res. B **98**, 122 (1995); D. L. Moores and K. J. Reed, Phys. Rev. A **51**, R9 (1995).
[14] D. L. Moores and K. J. Reed, J. Phys. B **28**, 4861 (1995).